Large Scale Simulation of Industrial, Engineering and Geophysical Flows Using Particle Methods

Paul W. Cleary, Mahesh Prakash, Matt D. Sinnott, Murray Rudman and Raj Das

Abstract Particle based computational methods, such as DEM and SPH, are shown to be widely applicable as tools to understand complex large scale particulate and fluid flows in industrial processing, civil, marine and coastal engineering and geohazards.

1 Introduction

DEM has been developed and used over the past 30 years for modelling flows of particulate solids in many applications, starting with small systems in simple geometries in two dimensions [1–4]. It is now possible to model systems of tens of millions of particles on desktop computers [5, 6] enabling many complex particulate flows to be explored in depth. It is the most effective method for any flow controlled by collision of particulates.

SPH is a powerful particle method that is suitable for solving complex multiphysics flow and deformation problems. It is particularly well suited to splashing free surface flows, interaction with dynamic moving bodies and discrete particles. It is also very well suited to situations where flow or material history is important. The method was first developed for incompressible flows by Monaghan [7]. Many examples of SPH applications are given in [8].

The inherent flexibility of these two Lagrangian techniques allows them to be easily and effectively applied to a wide range of different modelling problems with the only adjustments required being modifications to the detailed physics. In this chapter we describe a sub-set of the applications where such methods have been applied and highlight the diversity of physics and modelling scenarios that can be readily handled by DEM and SPH.

Paul W. Cleary · Mahesh Prakash · Matt D. Sinnott · Murray Rudman · Raj Das
CSIRO Mathematics, Informatics and Statistics, Private Bag 33, Clayton South, Victoria, 3168, Australia; e-mail: paul.cleary@csiro.au

E. Oñate and R. Owen (eds.), *Particle-Based Methods*, Computational Methods in Applied Sciences 25, DOI 10.1007/978-94-007-0735-1_3,

2 Industrial Flows

Industrial applications can be broadly classified according to their key physical processes, such as:

- Mixing (fluid, particulate and fluid-particulate)
- Separation
- Comminution
- Agglomeration
- Storage/unloading/transport
- Material forming (casting, forging, extrusion, forming, etc.)
- Sampling
- Excavation
- Fracture and material failure
- Bio-medical and biomechanical
- Fluid-particulate flow
- Fluid-bubble flow

In this section we will explore the use of particle based modelling in predicting the behaviour of these flow based processes.

2.1 Mixing

Mixing of granular materials occurs in applications as broad as minerals processing, chemical manufacture and pharmceutical preparation A variety of techniques have been developed to mix granular materials, often based on empiricism and intuition. This diversity is suggestive of a fundamental lack of rigorous understanding of granular mixing. DEM is an ideal technique for developoing such understanding.

A peg mixer is one example of a device that uses an agitator to mix a bed of particles. It is commonly used to reduce residence times and thus equipment dimensions compared to tumbling blenders and bins. In Figure 1 we study a laboratory-scale version. This peg mixer has a 300 mm diameter, 600 mm long cylindrical shell. Agitation is achieved using an axially mounted peg-agitator consisting of 18 pins attached to a 50 mm shaft and arranged at equal intervals along a helical path. Each pin is 15 mm in diameter and 125 mm in length with ends that move just inside the surrounding shell. The mixer rotates anti-clockwise at 60 rpm for a period of 30 seconds. Feed material enters the mixer through a 60 mm inclined port at the left end. The feed rate is chosen to match the discharge rate at the other end so as to ensure that the bed mass remains constant at 22 kg. The particles are spherical with density 2000 kg/m^3 and have a size range of 2.–8.8 mm. This is a collision dominated particulate system and consequently, DEM is the ideal technique to predict the flow behaviour. The particles have a coefficient of restitution of 0.3 and a friction coefficient of 0.75. A spring stiffness of 5000 N/m is used.

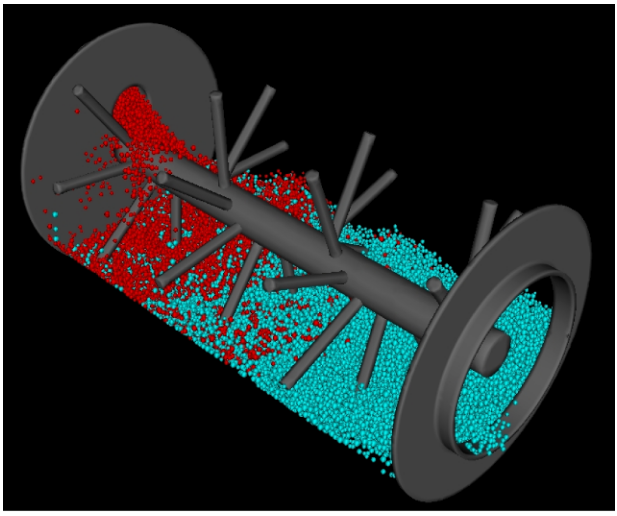

Fig. 1 Mixing in a continuously fed peg mixer predicted using DEM

Figure 1 shows the progress of feed material (red) through the original bed of particles (blue). The feed material falls onto the rotating shaft and is distributed over the bed near the feed opening. Particles are moved around by the axially migrating recirculation zones set up by the peg movement. Direct interaction with the pegs gives the particles high velocities leading to strong local mixing, particularly close to the surface of the bed where the impacts with the pegs can move individual particles a significant distance. In Figure 1 the feed material dominates the first quarter of the mixer with some particles having already passed the mid-point. The flow behaviour is quite different to the plug flow observed in a conventional drum mixer and the interface between the blue and red particles is much less sharp in the mixer here. The effect of design choices for the agitator on axial transport and agglomerate break-up can be assessed using DEM simulation. For more details on how to quantify mixing and for assessment of particulate mixing in many types of mixers using DEM [9].

Figure 2 shows the progress of the mixing and submergence of buoyant particulates into a fluid in a 1 m diameter cylindrical tank. Here the modelling is performed using SPH with the particulates modelled as clusters of SPH particles having a pellet-like shape.The impeller is downward pumping and its motion sets up a swirl in the tank with a downward axial flow at the impeller shaft that leads to a bulk recirculation within the tank. At 1.0 s, this downdraft begins to pull down the highly buoyant pellets. By 1.5 s, the pellets have started to cluster near the centre of the tank. By 2 s (Figure 2a) the pellets are starting to be dragged down into the fluid with the leading pellets reaching half way down the shaft. The recirculating flow pattern is fully established around 2.5 s and a significant proportion of the pellets have been drawn down towards the impeller. By 3.0 s, (Figure 2b) pellets are flung outwards by the impeller and are re-circulated within the fluid. Very good agreement is obtained with experiment for the distribution of solids, the critical speed for

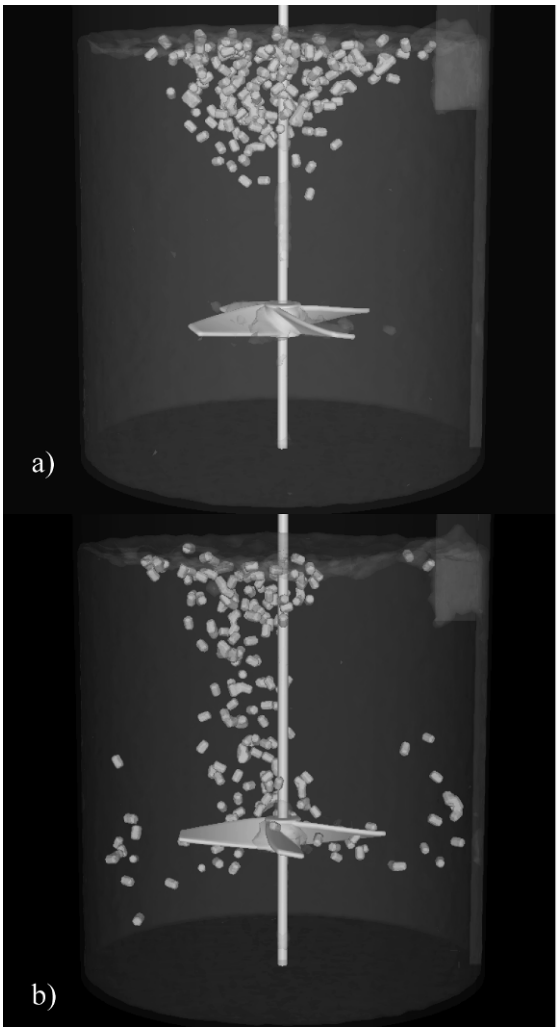

Fig. 2 Mixing and submergence of buoyant particulates in a tank of water driven by a central impeller rotating at 200 rpm, after (a) 2 s and (b) 3 s

submergence and the rate of submergence. This demonstrates that SPH is a viable method for predicting mixing of particulate-fluid systems. For the detailed comparison to experiment [10].

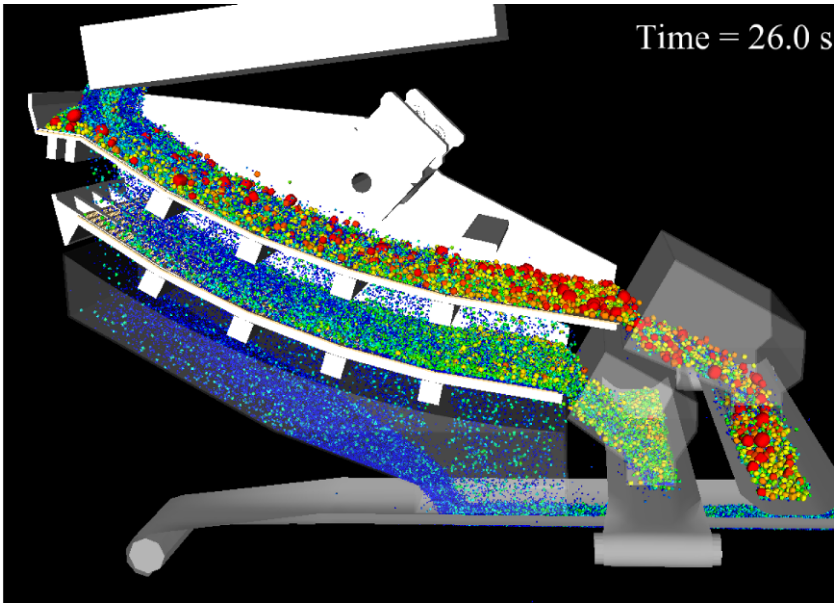

Fig. 3 Separation by a double deck banana screen with 5 g peak acceleration. The particles are coloured by size with red being coarse, green are the intermediate sizes and blue are the fines

2.2 Separation

Screens are often used for separation of particulates into different size fractions. They consist of one or more decks that are fitted with screen panels with arrays of square or rectangular holes. The screen is vibrated at high frequency to generate peak accelerations of 3–10 g which separates particles flowing over the screen according to size.

Material passing through the first and second panels of the top deck leads to the formation of a dense bed on the bottom deck. The blue (fine) material falls fairly quickly through the top deck bed so the visible particles are increasingly red to yellow in colour reflecting the ongoing removal of the fine material. The bed depth on the bottom deck increases along the screen as material falls from above and builds up. The colour of the lower deck bed changes from blue to green/yellow over the third and fourth panels again reflecting the removal of fines that fall through to the lower collection chute as an underflow stream. The contribution to the separation efficiency of each panel of each deck can be understood allowing the screen design and/or operating conditions to be optimized. For detailed analysis of the product size distributions, evaluation of the contribution of each panel to the separation of each deck and wear and power consumption [11, 12].

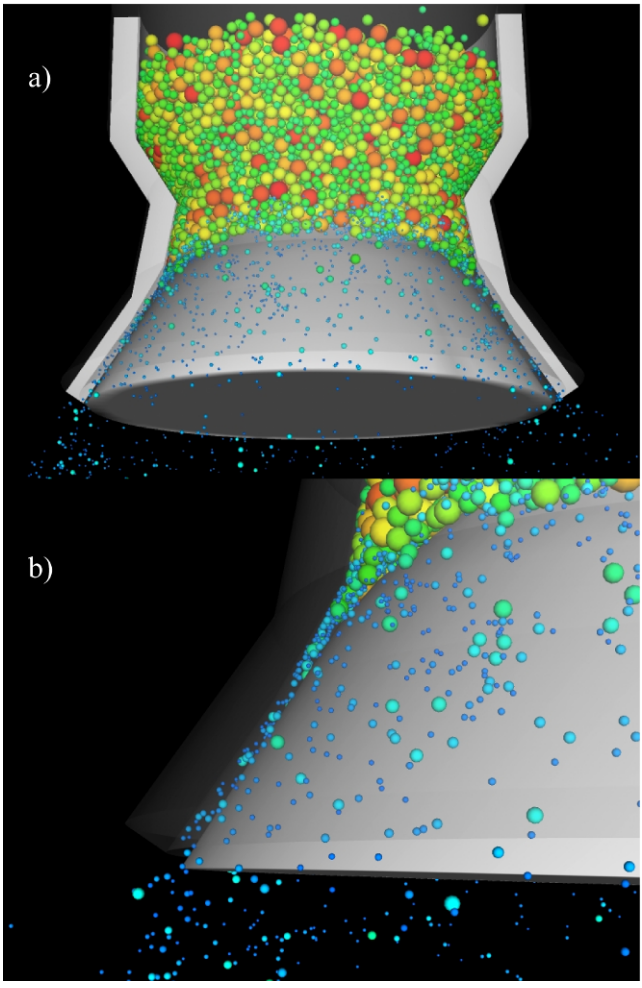

Fig. 4 Particle distribution in the cone crusher with particles coloured by size. The material is appreciably finer (blue) after passing the choke point of maximum constriction. The concave is the sectioned outer object and the mantle is the nutating conical object over which particles flow

2.3 Comminution

Comminution is the process of reducing the size of particles by breakage. It starts with large particles which are typically broken by one or more stages of crushing. The intermediate size particles produced are then fed to grinding mills that grind the particles down to mm or micron size. DEM simulations of a crusher and a mill are presented.

Figure 4 shows a DEM model of a cone crusher (around 0.6 m wide and 0.4 m high). The cone crusher is choke fed from above with medium size material (10–

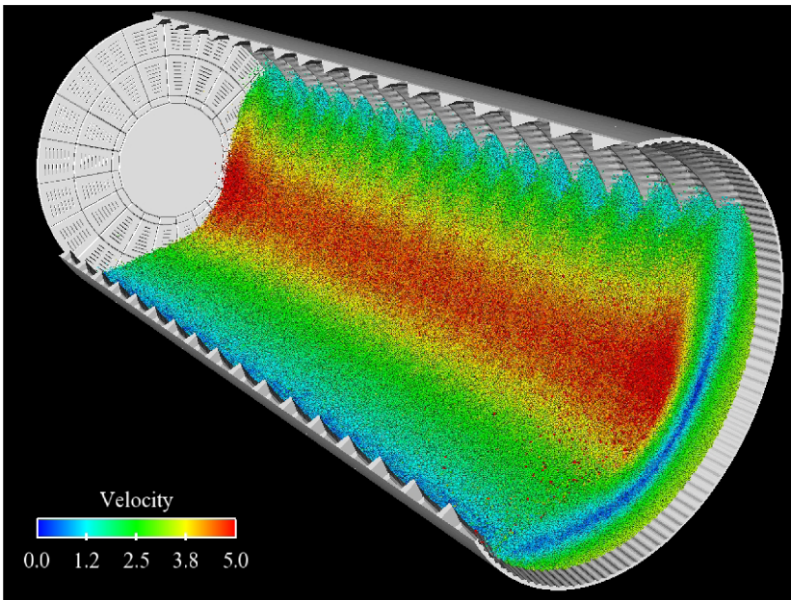

Fig. 5 Ball flow pattern in the second chamber of a cement mill. The particles are coloured by velocity with red being high (5 m/s) and blue being slow (< 1 m/s)

40 mm). The mantle (the moving conical section in the middle) is inclined at 1o and rotates with a nutating motion at 600 rpm. The concave (the outer object) is stationary. At any circumferential location the mantle oscillates away from and toward the concave causing particles to fall into the crushing zone and be compressed and fractured. The DEM model uses dynamic breakage of the particles (with a compression breakage rule) as described in [13]. This permits the coarse parent particles to break and the daughter particles to move lower in the crusher and be re-broken before exiting the crusher at the bottom. This allows prediction of key machine outputs, including the power draw which was 9.5 kW and the throughput of 11.5 tonnes/hr.

Grinding of clinker for cement production is often performed in a two chamber ball mill. In the first shorter chamber, raw clinker feed is ground with the product being transferred to the second longer chamber. Here smaller balls are used to grind the product material even finer. Figure 5 shows such a second chamber of a cement ball mill. It has an inner diameter of 3.85 m, is 8.4 m long and rotates at 16.13 rpm (75% critical speed). It has a classifying liner with a symmetric wave profile and 120 wave peaks around the circumference of the mill. The feed end of each lifter has a vertical step up to its highest point. The height then decreases along the lifter. There are 17 sets of these lifters along the axis of the mill. The ball size ranges from 15 to 50 mm and the fill level is 30% by volume, leading to a ball charge of 136.4 tonnes consisting of 3.2 million balls.

Figure 5 shows the charge motion in the mill with particles being dragged around by the mill shell to a shoulder position where they become mobile and flow down

as a cascading stream to the toe position. They are then re-captured by the liner and begin to circulate again. The free surface has the characteristic *S* shape. The particles move slowly near the shoulder and toe. As they flow down the surface they accelerate reaching peak speeds of 5 m/s in the steep central section. The particles near the mill shell are transported around with the mill rotation at speeds of close to 3 m/s. There is a narrow band of dark blue connecting the shoulder and toe. This material is very slow moving. Between the slow moving semi-circular blue band and the mill shell is a region of strong shear. Similarly, there is high shear between the slow moving layer and the high speed cascading flow above. Fine clinker particles are systematically trapped and crushed between the balls as they pass each other in these separate sliding layers.

2.4 Material Forming

SPH has been demonstrated to be a very effective method for predicting complex fluid flow in the High Pressure Die Casting (HPDC) process [14, 15]. Here we show the casting of an automatic differential cover. This component has a very complex three dimensional shape. The base plate is about 250 mm $\times$ 250 mm square in area. A thin-walled dome-like structure rises from the base plate and has an average section thickness of about 6.5 mm. Two cylindrical bosses blend into the dome and several bolt plates are raised from the surface to allow structural attachment to the car. Liquid aluminium is injected into the die cavity through the curved gates attached to one side of the base plate. The gates are are fed from a runner system attached to the shot sleeve. The liquid metal in the shot sleeve is pressurised by a plunger that forces the metal out into the runner system, through the gate and into the part. In this simulation an SPH particle size of 0.75 mm is used. When the cavity is completely filled, the total number of particles is about 900,000. The liquid aluminium viscosity used is 0.01 Pa s and the density is 2700 kg/m^3.

Figure 6 shows the filling pattern at 40 ms. Fluid initially enters the die at 10 ms, forming two broad jets at diverging 45° angles, partially fragmenting to spray across the cavity. In regions of die curvature, the wall drag causes the fluid to slow and the following fluid catches up leading to the formation of moderately coherent streams with fragmented boundaries. By 40 ms (Figure 6), almost the entire half of the die on the far side of the gate is filled and the detailed topographic structures are becoming clear. There is a strong back flow along the sides and along the base plate towards the gates. The dominant void regions are now just the areas on either side of the incoming streams from the gate, with some residual voids present on the top, behind the horizontal boss, and on the sides of the vertical boss. All the exit vents that are attached to the base plate are now blocked and all the remaining air in the die (represented here as the void regions) is trapped, leading to porosity formation. By 50 ms, there has been significant back filling as fluid flows back from the far side of the die to fill upcavities in the leading half of the die. Filling is complete after 60 ms with the last areas to fill being adjacent to the gates.

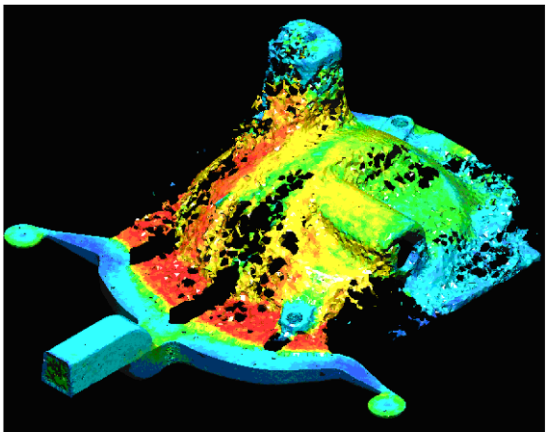

Fig. 6 Filling of a differential cover with the molten aluminium. The fluid is coloured by speed with blue being slow and red being fast

SPH is also well suited to simulating mechanical forming processes such as forging and extrusion due to its ability to model complex free surface behaviour, its ability to tolerate high levels of deformation and its history tracking capability. Here we show an SPH prediction of cold extrusion of aluminium alloy A6061 through a simple orifice. The initial billet dimension is 50 $\times$ 50 mm and the ratio of the extruded product width to the billet width is 1:2. A punch speed of 25 m/min is used for the simulation. An SPH particle separation of 1 mm is used giving a total of around 2,700 particles.

Figure 7 shows the progress of the billet being extruded. On the left material is coloured in vertical strata according to the initial material position so we can track internal deformation. On the right, the particles are coloured by their plastic strain. Once the billet corners contact the converging walls of the die, the metal quickly becomes elastically loaded and begins to undergo plastic deformation. By 20 ms, the leading edge of the billet has reached the end of the convergent section and mild plastic strains of up to 50% are found in these regions. By 60 ms, the leading edge emerges from the die. High strains of around 200% are observed in the regions just adjacent to the die walls. The distribution of plastic strain is fairly uniform along the length of the extruded rod but has significant variation across the width. The strong predisposition of the metal in the middle of the billet to flow preferentially along the centreline of the die is easily observed due to the frictional resistance of the walls. For more details about the application of SPH to solids forming processes [16].

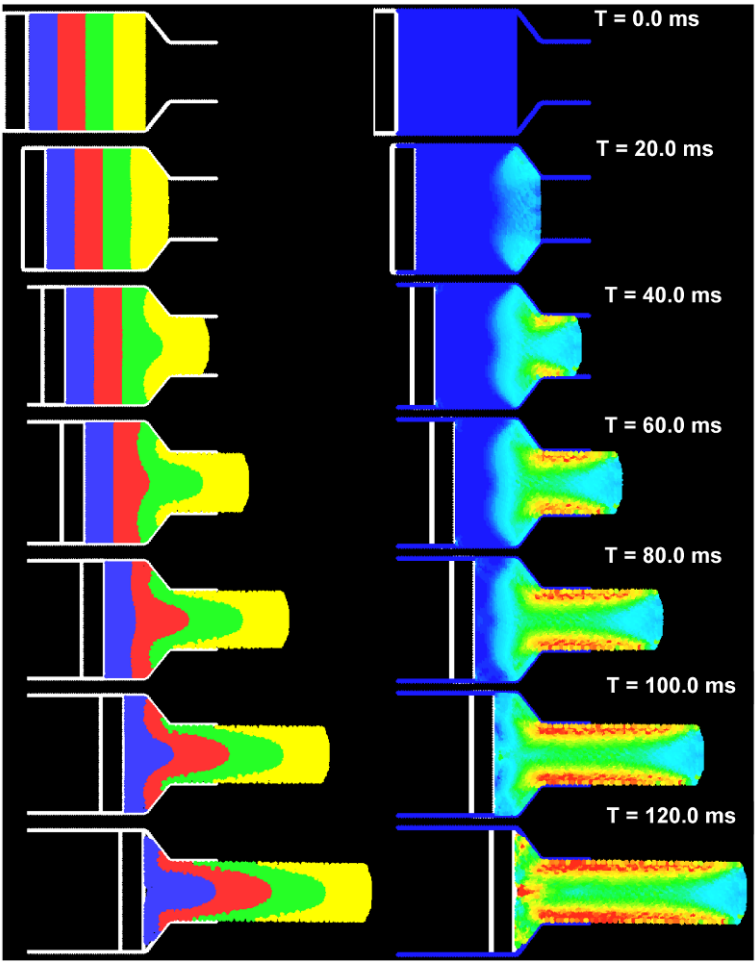

Fig. 7 Cold extrusion of aluminium using an elastoplastic SPH model. The particles are coloured (left) in four bands based on their initial position to show the deformation pattern and (right) by plastic strain with red being 1.8 and dark blue corresponding to 0.0

2.5 Bubbly and Reacting Multiphase Flows

Figure 8a shows a model of a bubbly flow, where bubbles are sparged into the fluid at the bottom. The fluid is modelled using SPH to enable prediction of the free surface and the oscillating gas source. The bubbles are represented as spherical discrete elements and can be created from either gas sources or a nucleation model. Nucleation sites are typically surface defects that dissolved gas diffuses to, creating bubbles via a phase change. Expanding bubbles evnetually separate from the surface, generating plumes of bubbles whose motions are coupled to the fluid flow [17] for details.

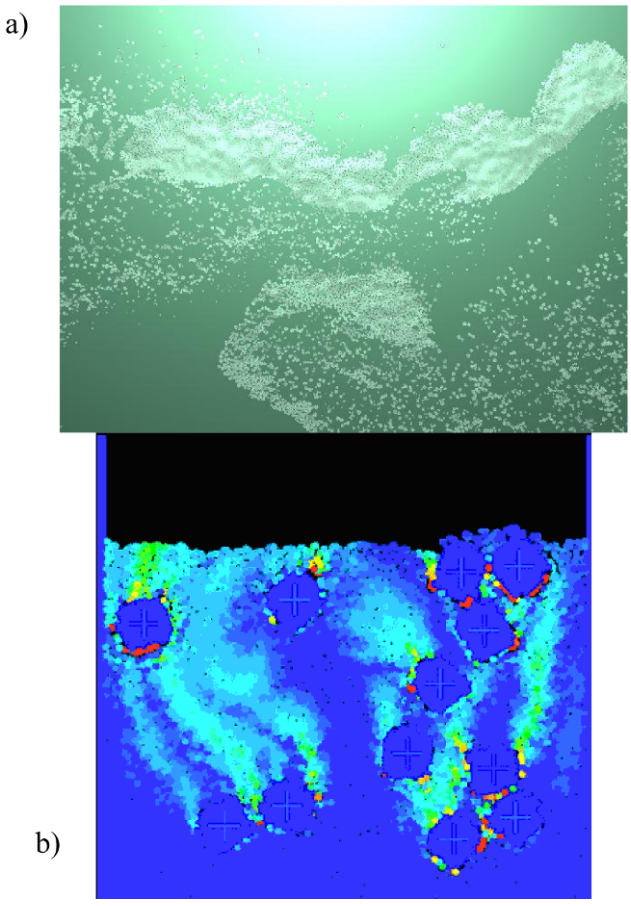

Fig. 8 (a) Bubbly flow with discrete bubbles coupled to an SPH flow, and (b) reacting particulates immersed in a hot liquid with fluid coloured by its volume fraction of reaction products

SPH can also be used to solve for thermal evolution [18] and for natural convective motion [19]. Combining these with the ability to model floating particles (see Figure 2) and the ability to predict the transport of the product gas through the liquid (including coupling of gas bouyancy into the fluid motion [8]) allows reacting multiphase flow to be modelled. Figure 8b shows the motion of bouyant reacting pellets in a liquid bath. The colour represents the volume fraction of product gas. It shows the generation of gas from the pellets and its transport through the liquid bath. The buoyant pellets float rapidly and cluster near the surface because they are positively buoyant. Note that the gas motion around and above each pellet creates a buoyant plume that tends to entrain fluid which in turn pushes the pellet upwards. So the natural buoyancy of the pellets is enhanced by the generation of buoyant gas plumes from the reacting pellets.

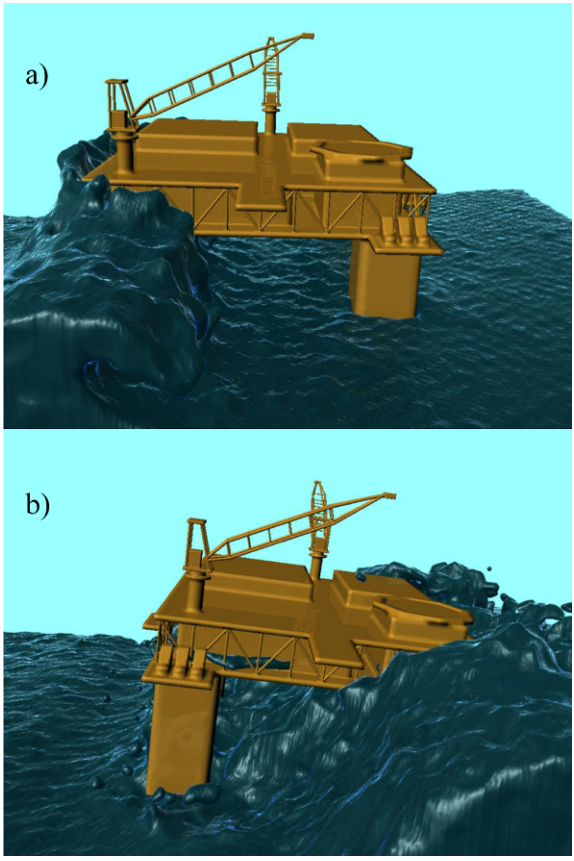

Fig. 9 Impact of a rogue wave on a 60 m high floating oil platform, after (a) 7.2 s and (b) 10.4 s

3 Fluid-Structure and Engineering Flows

Particle methods also provide powerful capabilities for modelling fluids and solids behaviour in civil, marine, ship and coastal engineering, construction and structural failure applications.

3.1 Rogue Wave Impact on an Moored Oil Platform

Figure 9 shows the impact of a 30 m rogue wave on a floating oil platform that is moored to the ocean floor using a Taut Spread Mooring (TSM) system. In Figure 9a, the wave can be seen approaching from behind. It is about 40 m away and just beginning to break with the top of the wave travelling in excess of 25 m/s. Wave impact starts at about 6 s, with contact occurring across the entire leading surface of

the platform. The top of the wave is just below the top deck. The extreme pressure of the water pushes the platform to the right (termed surge) and tilts it sharply clockwise (termed pitch). Figure 9b shows the platform at 10.4 s when the rogue wave has just passed the back of the platform. The surge at 15 m and the pitch of 8o are now substantial. Water splashing over the super-structure inundates much of the top of the platform. Over the next few seconds the platform starts to straighten with the pitch halving. The maximum surge has passed and the platform starts to move back to the left. The rogue wave has passed then beyond the platform, but the equally dangerous following trough is now directly under the platform. For more details of the recovery process and the comparative performance to other rigging systems and the effect of large conventional waves [20].

3.2 Ship Slamming and Green Water–Ship Interaction

The ability to easily couple free surface fluid motion to the dynamic response of objects subject to fluid forces is an attractive feature of the SPH technique. One important application is in the area of marine hydrodynamics where a range of different physical phenomena need to be captured. Two of these are known as "slamming" and "green water on deck" (see Figure 10).

Slamming occurs when the combination of swell position and pitch of the vessel causes the bow (or stern) to rise completely above the sea surface. As the pitch and swell change, the bow (or stern) can slam down onto the sea surface, giving rise to high pressures and structural loads that can damage the vessel structure. Green water on deck occurs in similar conditions to slamming and is caused when the pitch of the vessel causes the next wave to wash over its bow. This water is not in the form of spray or foam, instead being a large coherent volume of water, hence the term "green water". The volume and speed of the water mean that significant danger to crew arises and damage can be done to the deck, the superstructure and infrastructure such as lifeboats. Green water can also take a long time to drain from the deck, temporarily increasing the weight and behaviour of the vessel and decreasing manoeuvrability.

3.3 Spillway Flow and Dam Discharge

Spillways are structures used for the controlled release of water from a dam or levee into a downstream area, typically the river that was dammed. Spillways release flood waters so that the water does not overtop and damage, or even destroy, the dam. As flow through a spillway involves complex free surface behaviour SPH is a very attractive method for such modelling. Figure 11 shows flow into a spillway from four open gates using approximately 500,000 fluid particles with a resolution of 25 mm. Figure 11a shows the initial release as the front just leaves the spillway

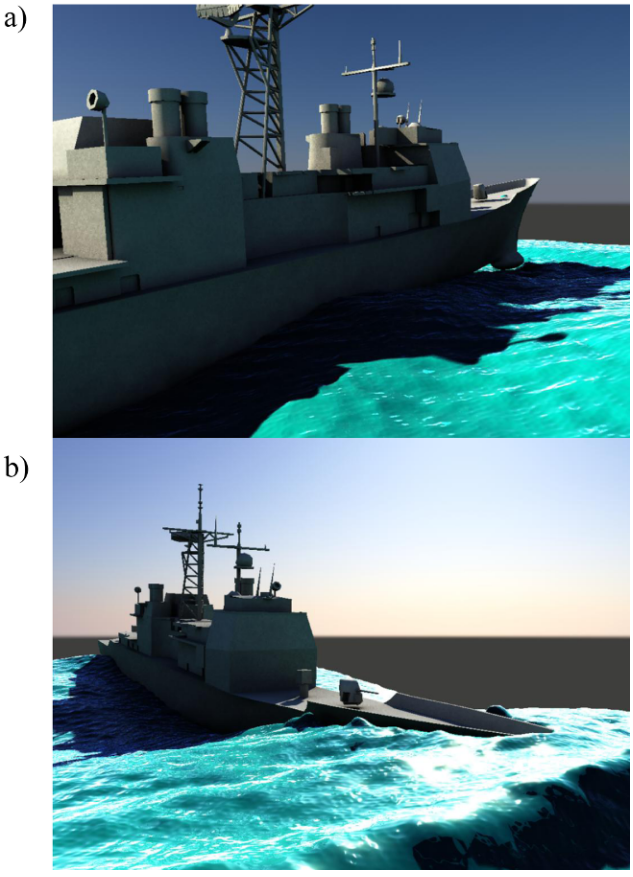

Fig. 10 SPH simulation of a Ticonderoga-class cruiser travelling at 20 knots in a 6 m swell. In (a) the bow of the ship is completely above the sea surface and is about to "slam" down onto it. In (b) the bow has dipped significantly after the slamming event and has dug into the next wave in the swell, leading to green water washing over the deck

structure. The steady state flow is reached after 2.5 min of the opening of the gates and is shown in Figure 11b.

3.4 Dam Wall Collapse under Earthquake Loading

Dam failures are catastrophic and create significant economic loss and loss of human life. A common cause of failure is the cracking that results from seismic load, uneven settling of foundations, and thermal and residual stresses. Fracture of the Koyna dam subjected to earthquake-type motion is modelled using an elastic brittle SPH formulation [21], and the fracture pattern is shown in Figure 12.

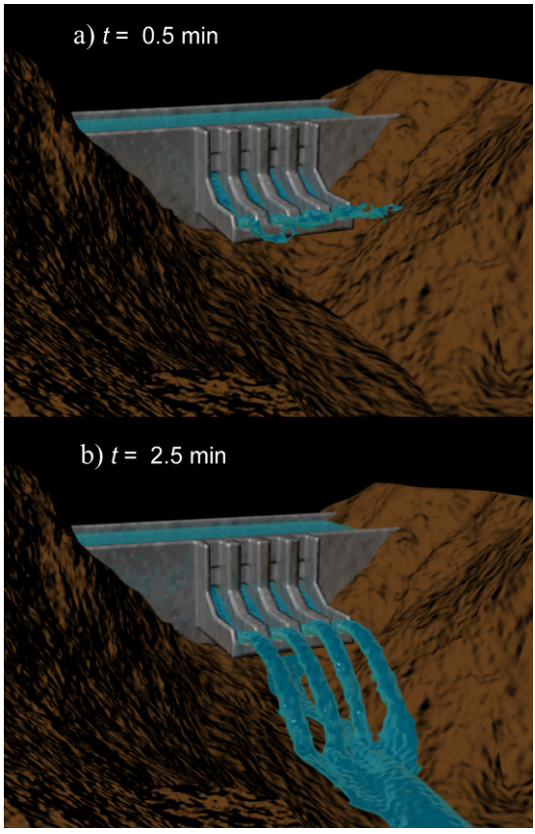

Fig. 11 Discharge of water from a dam and flow down the spillway

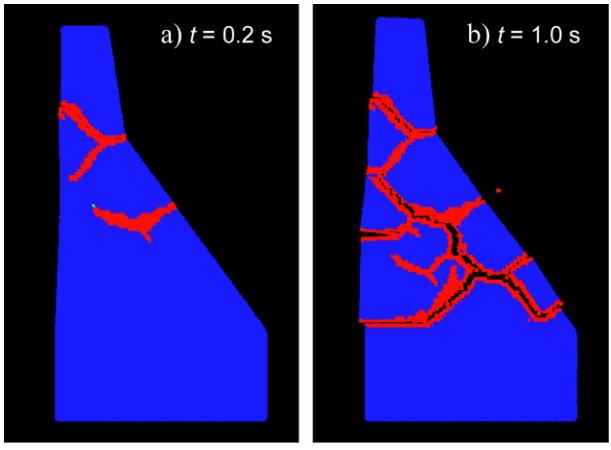

Fig. 12 Fracture pattern of the dam subjected to base motion in the horizontal and vertical directions (coloured by damage with blue being no damage and red being fully fractured)

The base of the dam is subjected to fluctuating loads in the horizontal and vertical directions to simulate the ground motion during an earthquake. The cracks originate normal to the wall surface, because the tangential stress is approximately equal to the maximum principal stress near the free surface. As the cracks propagate towards the interior, they branch one or more times to produce pairs of cracks in each branch. These new cracks propagate towards the surfaces of the dam structure because this provides the path of least resistance to fracture. During the periodic dynamic loads, the interaction of the impinging stress waves with the rarefaction compression waves reflected from the free surfaces slows the normal propagation of cracks. So as the crack front approaches the free surface it decelerates causing bending of the advancing crack front. This is observed for the uppermost crack on the left face and the lowermost crack on the right face in Figure 12b. This phenomenon is known as 'crack arrest'. The patterns are qualitatively similar to those observed in practice [22].

3.5 Fracture of a Structural Column during Projectile Impact

Brittle fracture of slender structures under impact has importance in many applications, such as high-speed weapons systems, impact resistant buildings, and extreme geophysical events. Here we use SPH to investigate the collision of a high speed projectile with a stationary column. Figure 13 shows the fracture of a stationary concrete column when hit by a steel projectile travelling from right to left at a velocity of 125 m/s. Figure 13a shows the onset of fragmentation. Two distinct regions can be identified based on the level of fragmentation: the completely damaged central region with debris/fine particles and the larger fragments above and below this debris zone. The debris cloud erupts horizontally from the left face of the column, leading to its catastrophic failure (Figure 13b). The front of the debris cloud is flat with projections near the ends, and the rear is conical in shape due to the inclined primary fracture planes. Near the top and bottom ends of the column, there are regions of low stress surrounded by cracks (non-red regions in Figure 13b) which show the secondary fracture planes that become fragmentation boundaries.

3.6 Excavation

Excavation is an important part of mining and construction. The digging of rocks by moving machinery is well modelled using DEM [23]. Figure 13 shows the filling sequence for an ESCO bucket with non-spherical particles ranging in size from 100 to 300 mm. As the bucket moves towards the dragline, the lip and teeth bite into the overburden, producing an initially thin stream of particles flowing into the bucket. As it fills, the resistance to shear of the material already in the bucket needs to be overcome in order for the material to be pushed up into the back of the bucket. A pile

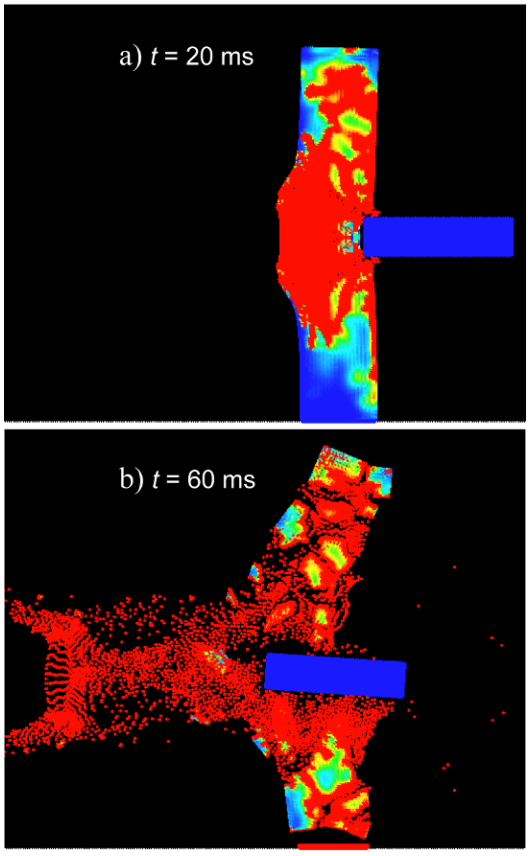

Fig. 13 Fracture pattern of the column and fragment distribution after collision for an elastic projectile (coloured by damage with blue-red corresponding to damage range 0–1)

of particles forms in front of the bucket that is of comparable height to the particles in the bucket. This pile is bulldozed along in front of the bucket. Its size increases until the resistance to shear of this pile exceeds the resistance of the material inside the bucket causing it to flow and increase in volume and therefore height. Once the bucket is substantially filled the drag process is complete. The front cables shorten, the bucket lifts and the rock is removed. The drag cycle for this rock material takes 12 s.

4 Geo-Hazard and Extreme Geophysical Flows

Geo-hazard or extreme flow events are abrupt, large scale motions of particulate solids and/or fluids. They can generate significant loss of life and economic damage.

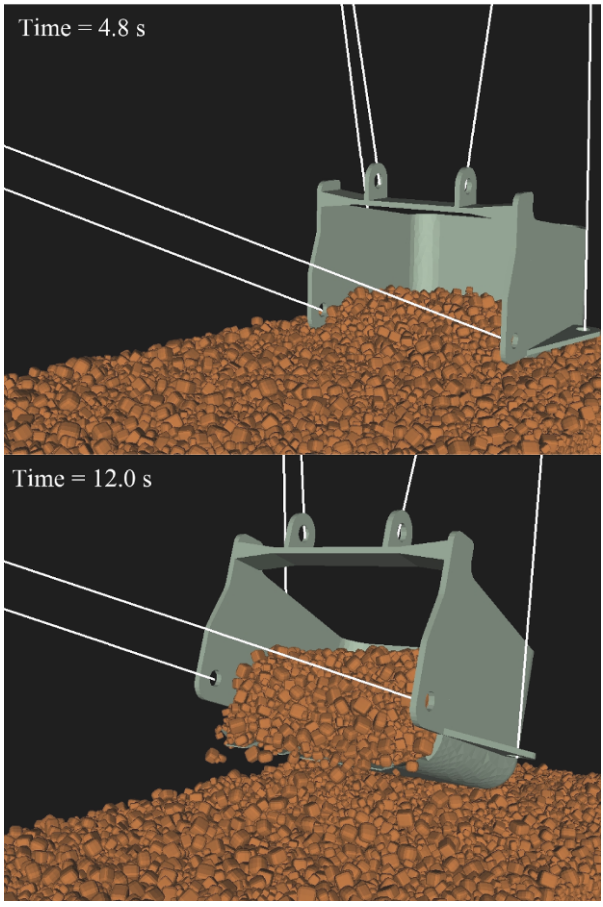

Fig. 14 Progress in the filling and lifting of an ESCO dragline bucket for a non-spherical rock overburden with a 100 mm bottom particle size

They include landslides, debris flows, flooding induced by extreme rain and dam collapse, storm surge, tsunamis, pyroclastic flows and volcanic lava flows. Computational modelling of extreme rock and fluid flow events, such as landslides and dam collapses, can provide increased understanding of their post-initiation course. This can provide valuable insight into opportunities for designing mitigation strategies and to enable more informed management of such disaster scenarios. For the prediction of fluid based geo-hazards such as dam breaks SPH is ideally suited to predicting the resulting complex, highly three dimensional, free surface flows. These flows involve splashing, fragmentation, and interaction with complex topography and engineering structures [24]. For landslides, which are collision dominated flows of rocks, DEM provides an ideal method for prediction [5, 6, 24–26].

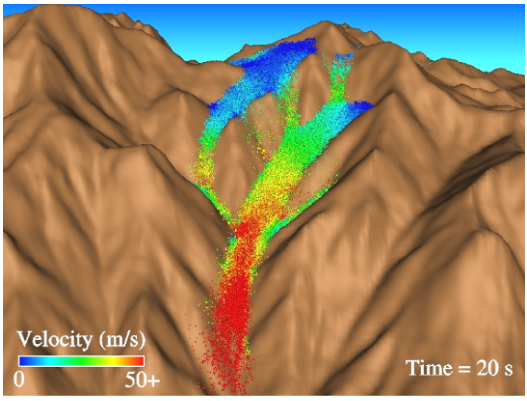

Fig. 15 Landslide from a collapsing mountain peak with particles coloured by velocity

4.1 Landslide

Figure 8 shows the collapse of the mountain peak into a valley. The particles are coloured by their speed with blue being stationary and red being 50 m/s or higher. The initial peak was converted into a mound of non-spherical particles that are then free to flow on the underlying topography. The mass of rock in the landslide is 12 million tonnes. This represents a volume of 3.04 million m^3 and consists of 245,000 particles. The particle diameters are between 2.0 m and 10.0 m with a mean diameter of 2.4 m. They collapse forwards and down two side valleys producing a left and right branch of the landslide, which are separated by a series of small peaks. By 20 s, the three branches all merge to create a single large flow of particles down the central valley. By 26 s, the supply of new material from the original peak location has slowed and the main landslide is moving at its peak speed and is approaching the valley floor where it comes to rest.

4.2 Flooding from Dam Wall Collapse

The St Francis Dam, located in the San Francisquito Canyon, about 15 km north of Santa Clarita, California, failed on 12 March 1928 and at least 450 people were killed in the resulting floods. The dam wall was 57 m high, 213 m long and at the time of failure contained 47 million mş of water. Here we show an SPH prediction of the scenario involving instantaneous collapse of the sections of the dam wall that failed. Within 10 s the leading water has collapsed and travelled around 200 m into the canyon. In the shallow valley just beyond the dam wall the flood front has a parabolic shape and is deeper and faster in the middle. By 1 min the flood front has travelled 0.5 km from the dam wall and has reached the opposite side of the valley. The water speed across most of the valley floor is around 20 m/s. By 2 min

(see Figure 16) the water stretches across a region approximately 1.2 km wide in the main valley. The SPH method is able to capture important 3D flow structures as water flows from the dam breach and criss-crosses the valley downstream resulting in hydraulic jumps that are generated by irregularity in the real surface topography. The momentum of the flood water presses the water up against the right wall of the canyon which records the highest flood levels. The water then flows along this wall until it separates from the sharp bend in the foreground of this frame. The water then flows back across the now narrow canyon to the left wall where it is again reflected creating a smaller hydraulic jump diagonally across the valley. Water begins to enter the large flatter side valley on the left in the foreground. The flooding of two of the earlier side valleys is now well advanced. Figure 16 shows the flooding at 4 min after the failure. The predicted arrival time for the flood front at a power generation station using SPH is 3.5 min, which is close to the observed value of 4.5 min (taking account of the time needed to flood the station following the arrival of the water).

4.3 Tsunami

A tsunami is one or more waves generated in a body of water by an impulsive disturbance that vertically displaces the water. Earthquakes, landslides, volcanic eruptions and explosions can generate tsunamis. Tsunamis can savagely attack coastlines, causing devastating property damage and loss of life. The extent of the damage depends on the strength of the tsunami wave its angle of attack on the coastline and the bathymetry of the near shore region. Thus, the prediction of these waves can prove to be extremely useful in minimising the loss of life and property.

Here SPH is used to predict the impact of a tsunami wave as it approaches a coastline. Approximately 3 million fluid and 700,000 boundary particles are used. The fluid resolution is 3.5 m. The boundary has a resolution of 7 m. A tsunami wave with a speed of 30 m/s and a wave height of 45 m is shown approaching the coast in Figure 17a.The incident wave indundates the valleys and travels inland about 1 km in the first minute. Figure 17b shows the water middle stages of the inundation process. Here the leading water in the valleys is still travelling inland, but water closer to the coast is already flowing back into the ocean. The return wave that has been reflected off the shore line has significant structure reflecting the topographic complexity of the coast line.

5 Conclusions

DEM, SPH and their combination have been shown to successfully simulate fluid and collisional based particulate flows, multiphase flows (fluid-particulate and fluid-bubble flows), elastoplastic deformation and elastic-brittle failure of solids. Consequently they can be used to model challenging applications such as industrial

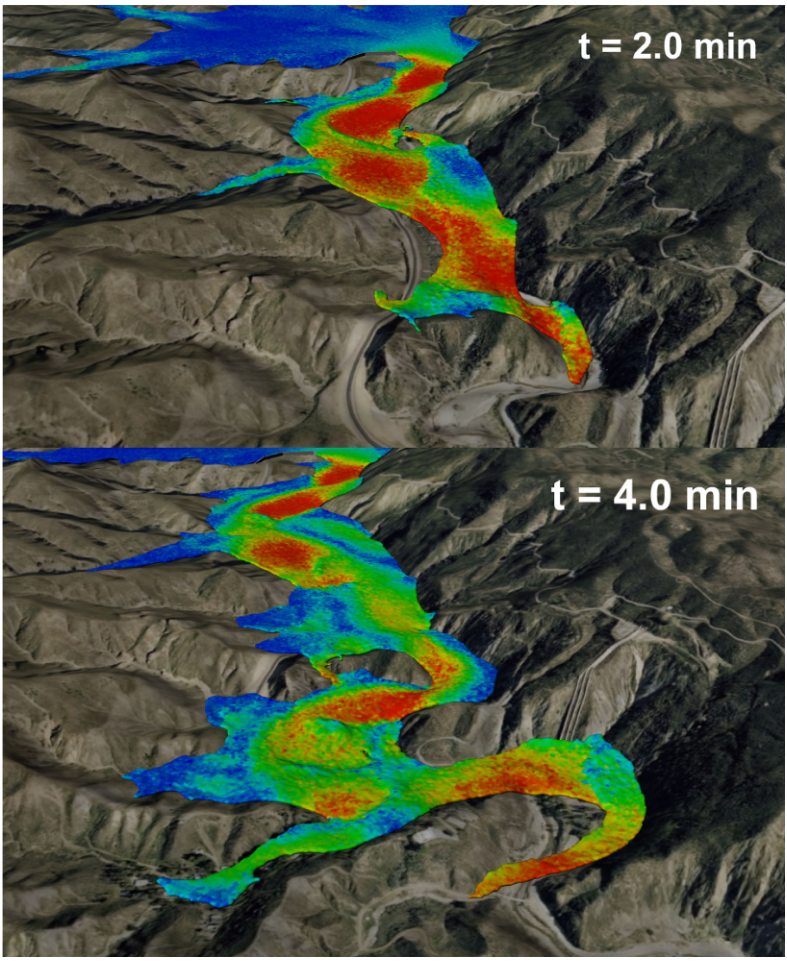

Fig. 16 Flooding following the collapse of the St Francis dam at (top) 2 min, and (bottom) 4 min after the collapse

processing, civil, marine and coastal engineering, fluid-structure interaction and extreme geophysical flows. The methods provide robust tools that can be used to understand complex flow processes and as part of design and optimisation of processes and equipment and for risk and mitigation strategy evaluation.

Acknowledgements

The modelling of the banana screen was carried out under the auspice and with the financial support of the Centre for Sustainable Resource Processing, which is

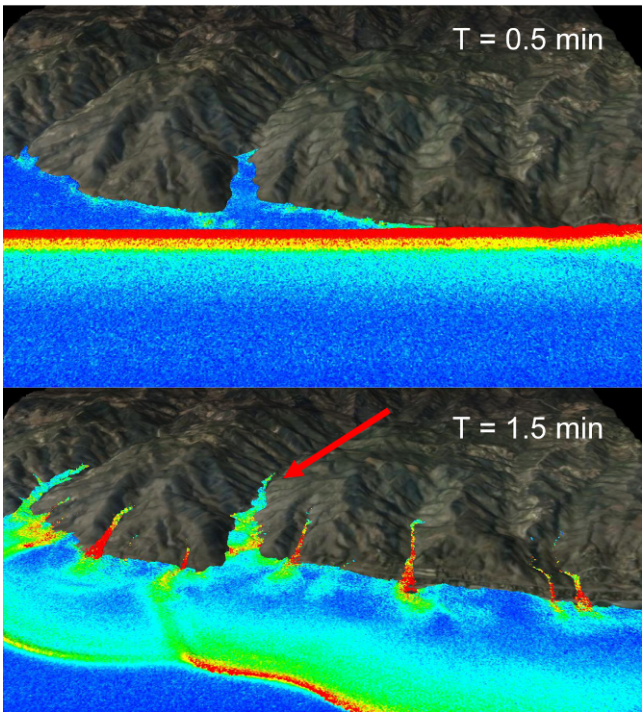

Fig. 17 Incoming linear tsunami wave (top) and aftermath one minute later (bottom) with retreating waves and inundation of valleys and low lying areas. Fluid is coloured by speed with red being high (30 m/s) and dark blue being stationary

established and supported under the Australian Government's Cooperative Research Centres Program.

The authors wish to thank their collaborators at ETRI (South Korea) for their contribution to the SPH-DEM bubble modelling.

References

1. Cundall, P.A., Strack, O.D.L., A discrete numerical model for granular assemblies. *Geotechnique*, 29:47–65, 1979.
2. Walton, O.R., Numerical simulation of inelastic frictional particle-particle interaction (Chapter 25). In: *Particulate Two-phase Flow*, M.C. Roco (ed.), pp. 884–911, 1994.
3. Campbell, C.S., Rapid granular flows. *Annual Review of Fluid Mechanics* 22:57–92, 1990.
4. Haff, P.K., Werner, B.T., *Powder Technology* 48:239, 1986.
5. Cleary, P.W., Large scale industrial DEM modelling. *Engineering Computations* 21:169–204, 2004.
6. Cleary, P.W., Industrial particle flow modelling using DEM. *Engineering Computations* 26:698–743, 2009.

7. Monaghan, J.J., Simulating free surface flows with SPH. *Journal of Computational Physics* 110:399–406, 1994.
8. Cleary, P.W., Prakash, M., Ha, J., Stokes, N., Scott, C., Smooth particle hydrodynamics: Status and future potential. *Progress in Computational Fluid Dynamics* 7:70–90, 2007.
9. Cleary, P.W., Sinnott, M.D., Assessing mixing characteristics of particle mixing and granulation devices. *Particuology* 6:419–444, 2008.
10. Prakash, M., Cleary, P.W., Noui-Mehidi, M.N., Blackburn, H., Brooks, G., Simulation of suspension of solids in a liquid in a mixing tank using SPH and comparison with physical modeling experiments. *Progress in Computational Fluid Dynamics* 7:91–100, 2007.
11. Cleary, P.W., Sinnott, M.D., Morrison, R.D., Separation performance of double deck banana screens – Part 1: Flow and separation for different accelerations. *Minerals Engineering* 22:1218–1229, 2009.
12. Cleary, P.W., Sinnott, M.D., Morrison, R.D., Separation performance of double deck banana screens – Part 2: Quantitative predictions. *Minerals Engineering* 22:1230–1244, 2009.
13. Cleary, P.W., Recent advances in DEM modelling of tumbling mills. *Minerals Engineering* 14:1295–1319, 2001.
14. Cleary, P.W., Ha, J., Ahuja, V., High pressure die casting simulation using smoothed particle hydrodynamics. *International Journal on Cast Metals Research* 12:335–355, 2000.
15. Cleary, P.W., Ha, J., Prakash, M., Nguyen, T., 3D SPH flow predictions and validation for high pressure die casting of automotive components. *Applied Mathematical Modelling* 30:1406–1427, 2004.
16. Cleary, P.W., Prakash, M., Ha, J., Novel applications of SPH in metal forming. *Journal of Materials Processing Technology* 177:41–48, 2006.
17. Cleary, P.W., Pyo, S.H., Prakash, M., Koo, B.K., Bubbling and frothing liquids. *ACM Transaction on Graphics* 26, Article No. 97, 2007.
18. Cleary, P.W., Monaghan, J.J., Conduction modelling using smoothed particle hydrodynamics. *Journal of Computational Physics* 148:227–264, 1999.
19. Cleary, P.W., Modelling confined multi-material heat and mass flows using SPH. *Applied Mathematical Modelling*, 22:981–993, 1998.
20. Cleary, P.W., Rudman, M., Extreme wave interaction with a floating oil rig: Prediction using SPH. *Proc. CFD* 9:332–344, 2009.
21. Das, R., Cleary, P.W., Effect of rock shapes on brittle fracture using smoothed particle hydrodynamics. *Theoretical and Applied Fracture Mechanics* 53:47–60, 2010.
22. Lee, O.S., Kim, D.Y., Crack-arrest phenomenon of an aluminum alloy. *Mechanics Research Communications* 26:575–581, 1999.
23. Cleary, P.W., The filling of dragline buckets. *Mathematical Engineering in Industry* 7:1–24, 1998.
24. Cleary, P.W., Prakash, M., Smooth particle hydrodynamics and discrete element modelling: Potential in the environmental sciences. *Philosophical Transactions of the Royal Society of London A* 362:2003–2030, 2004.
25. Cleary, P.W., Campbell, C.S., Self-lubrication for long run-out landslides: Examination by computer simulation. *Journal of Geophysical Research* 98(B12):21911–21924, 1993.
26. Campbell, C.S., Cleary, P.W., Hopkins, M.A., Large scale landslide simulations: Global deformation, velocities and basal friction. *Journal of Geophysical Research* 100(B5):8267–8283, 1995.